Efficient and readily tuneable near-infrared photodetection up to 1500 nm enabled by thiadiazoloquinoxaline-based push–pull type conjugated polymers

DOI: 10.1039/d0tc01435d
Handle: http://hdl.handle.net/1942/32695

Efficient and readily tuneable near-infrared photodetection up to 1500 nm enabled by thiadiazoloquinoxaline-based push-pull type conjugated polymers

Frederik Verstraeten[a,b,†], Sam Gielen[a,b,†], Pieter Verstappen[a,b], Jorne Raymakers[a,b], Huguette Penxten[a], Laurence Lutsen[b], Koen Vandewal[a,b], Wouter Maes[a,b,*]

[a] UHasselt – Hasselt University, Institute for Materials Research (IMO), Agoralaan 1 – Building D, 3590 Diepenbeek, Belgium

[b] IMEC, Associated Lab IMOMEC, Wetenschapspark 1, 3590 Diepenbeek, Belgium

[†] These authors contributed equally.

Abstract

The majority of bulk heterojunction near-infrared organic photodetectors (NIR-OPDs) have an absorption window up to 1000 nm (1.2 eV) due to the scarcity of suitable NIR-absorbing electron donor polymers and the challenging energy alignment and/or blend miscibility with electron acceptor materials, strongly complicating to move beyond this wavelength range. Nonetheless, extension of the detectivity further into the NIR is important for applications such as bio-imaging, pulse oximetry and industrial sorting. Herein, we illustrate that [1,2,5]thiadiazolo[3,4-*g*]quinoxaline (TQ) is an excellent building block for the development of ultra-low bandgap copolymers to achieve tuneable NIR photodetection beyond 1000 nm. Three TQ monomers with different side chain patterns are synthesized and combined with carefully selected electron rich subunits to yield push-pull type copolymers with an optical gap ranging from 1.14 to 0.87 eV. The highest gap material affords the best OPD performance, with a peak specific detectivity of $3x10^{11}$ Jones at 960 nm (at -2 V bias). The other polymers show sub-1 eV optical gaps and specific detectivities exceeding 10^{10} Jones up to 1400 nm (at -2 V bias). These values are among the highest reported so far for NIR-OPDs in the wavelength range beyond 1000 nm.

Introduction

The implementation of organic semiconductors in photodetectors has attracted worldwide interest, both from academia and industry, as they afford light-weight and flexible devices that can easily be produced on a large scale *via* printing technologies.[1–4] Additionally, the synthetic versatility of organic photoactive materials allows fine-tuning of the optoelectronic and physicochemical properties to the desired device specifications.[5–8] For a long time, the performance of organic photodetectors (OPDs) lagged behind that of the conventional inorganic ones. However, recent breakthroughs illustrate that OPDs are competitive now in the visible regime. For example, Kielar *et al.* reached a detectivity exceeding 10^{13} Jones in the spectral window of 350−650 nm with an impressively low dark current density of 0.3 nA/cm^{-2} (at -2 V bias), approaching the performance of Si photodetectors. Moreover, the devices were shown to withstand 14,000 hours of continuous operation.[9] For the near-infrared (NIR) region, beyond the detection limit of Si (> 1 µm), an alternative for the commonly used (epitaxially grown) InGaAs or HgCdTe photodetectors is desired because of their high cost, limited pixel size and high rigidity (e.g. detrimental for wearable applications).[3,10,11] Indeed, many applications could benefit from the development of efficient, flexible and cheap NIR-OPDs, such as night vision, industrial sorting, pulse oximetry and life science applications such as bio-imaging in the second NIR window (between 1000 and 1350 nm).[12–18]

To date, a very limited amount of well performing NIR-OPDs have been reported, from which most have external quantum efficiencies (EQEs) with a maximum (far) below 900 nm.[19–27] Photodetectors with a high detectivity beyond 1000 nm are scarce due to the limited amount of organic semiconductors with a sufficiently low optical gap.[28–32] In previous work, we have shown that push-pull copolymers based on bay-annulated indigo (BAI) are suitable for photodetection beyond 1000 nm with a (shot-noise limited) detectivity of approximately 10^{12} Jones (at -2 V bias) within the spectral window of 600−1100 nm.[33] For the detection of longer wavelengths, one often relies on push-pull type alternating copolymers composed of even stronger electron withdrawing subunits such as thieno[3,4-*c*][1,2,5]thiadiazole, thienoisoindigo, benzo[1,2-*c*;4,5-*c'*]bis[1,2,5]thiadiazole or [1,2,5]thiadiazolo[3,4-*g*]quinoxaline.[28,34–36] The latter building block, from now on referred to as TQ, combines the electron deficient thiadiazole and quinoxaline moieties and allows straightforward addition of solubilizing alkyl side chains.[36–38] The TQ monomer was applied in organic photovoltaics by Andersson *et al.* in 2007, affording a photoresponse up to 1200 nm, further extended to 2000 nm in 2014.[39,40] Its first application in push-pull copolymers for NIR-OPDs was reported in 2017 by London *et al.*, who managed to get a photoresponse between 600 and 1500 nm with a maximum detectivity of 3 x 10^{11} Jones at 1200 nm. Z. Wu *et al.* later on optimised the device leading to a remarkable peak EQE of 26% and a detectivity of 1.2 x 10^{11} Jones at 1100 nm with a photoresponse up to 1400 nm.[36,37] Although these results are outstanding, it should be noted that the detectivities mentioned above were determined at 0 V bias while typical readout schemes use reverse biases (e.g. -2 V) at which the response speed and linearity are significantly higher.[8]

Herein, we report a series of seven TQ-based push-pull copolymers and their implementation in prototype NIR-OPDs. Careful selection of the electron rich (push) subunits allowed proper tuning of the optical gap, leading to a photoresponse ranging from 1000 to 1500 nm. Combination of the TQ monomer with a rather weak push unit (phenyl) resulted in a polymer with a rather high optical gap of ~1070 nm. Due to this relatively high gap, quite low dark currents could be achieved when applied in NIR-OPDs, leading to a detectivity (at -2 V bias) exceeding 10^{11} Jones in the spectral region of 400−1050 nm. Copolymerization of TQ with more electron rich moieties caused a strong red-shift of the polymer absorption, now covering the NIR region from 800 up to 1400 nm. Although the reduction of the gap impacts the dark current density of the OPD devices, detectivities above 10^{10} could still be achieved up to 1400 nm (under -2 V bias).

Results and discussion

TQ is a very versatile building block for the development of NIR-absorbing conjugated polymers. It offers several advantages compared to other strongly electron deficient moieties such as BAI and thieno[3,4-*c*][1,2,5]thiadiazole.[33,34,36] For example, the synthesis route for TQ monomers is more straightforward and, more importantly, all synthesis steps afford relatively high yields (mostly above 70%) and the synthetic procedures can easily be scaled up (as purifications are often done by distillation or recrystallization). Furthermore, TQ can easily be functionalized at the pyrazine subunit with solubilizing alkyl side chains, ensuring polymer solubility for combinations with a wide range of electron rich monomers. To enable 2D conjugation, in this study, the TQ unit was decorated with alkyl bearing thiophene side groups. Three different TQ monomers with increasing alkyl side chain lengths were prepared, i.e. **TQ_{BO}**, **TQ_{HD}** and **TQ_{OD}**, containing 2-butyloctyl, 2-hexyldecyl and 2-octyldodecyl side chains, respectively. Variation in alkyl chain length is known to have a profound effect on the solubility of the resulting polymers and consequently also on the film forming properties and morphology of the bulk heterojunction active layer.[41–43] The synthesis procedures are outlined in **Scheme 1**, while additional details and characterization data are provided in the Electronic Supplementary Information file. In short, the side chain alcohol end groups were first converted to iodine groups to allow facile attachment to the 2-position of thiophene. Consecutive reaction with oxalyl chloride yielded dione derivatives **3**. In parallel, nitration of 4,7-dibromobenzo[*c*]-1,2,5-thiadiazole with fuming nitric acid, followed by Stille cross-coupling with thiophene, generated product **5**, which was further reduced with Fe into precursor **6**. Then, condensation between derivatives **3** and compound **6** afforded the TQ cores, which were brominated to form the final TQ derivatives **8**.

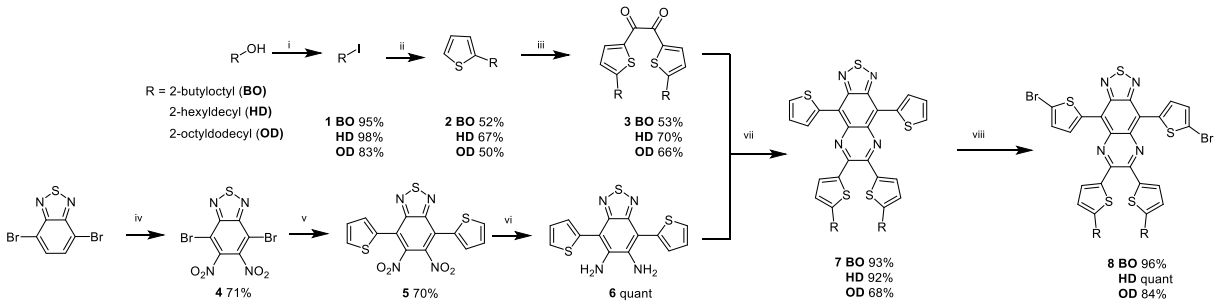

Scheme 1. *Synthetic pathway towards the TQ monomers: i) imidazole, PPh_3, I_2, THF, RT; ii) thiophene, n-BuLi, THF, -78 °C to reflux; iii) oxalyl chloride, $AlCl_3$, pyridine, CH_2Cl_2, RT; iv) fuming HNO_3, triflic acid, 50 °C; v) 2-tributylstannylthiophene, $Pd(PPh_3)_2Cl_2$, toluene/DMF, 125 °C; vi) Fe, AcOH, 80 °C; vii) AcOH, 125 °C; viii) NBS, $CHCl_3$, RT.*

These monomers were then polymerized with common (even commercially available) electron rich monomers based on thiophene (**T**), thieno[3,2-*b*]thiophene (**TT**), bithiophene (**BiT**) or benzene (**B**) (**Figure 1**). For the thiophene-based monomers, the conventional Stille cross-coupling polymerization was used, whereas the **PBTQ(BO)** polymer was synthesized *via* Suzuki polymerization.[44] The solubility, and hence processability, of the polymers was in line with the rigidity and stacking tendency of the electron donating monomers. The fused thienothiophene and benzene monomer only afforded soluble polymers when copolymerized with **TQ_{OD}**, resulting in **PTTTQ(OD)** and **PBTQ(OD)**. The less rigid bithiophene monomer afforded **PBiTTQ(HD)** and **PBiTTQ(OD)** as nicely soluble and processable polymers. Likewise, three processable polymers – **PTTQ(BO)**, **PTTQ(HD)** and **PTTQ(OD)** – were prepared from the distannylated thiophene monomer.

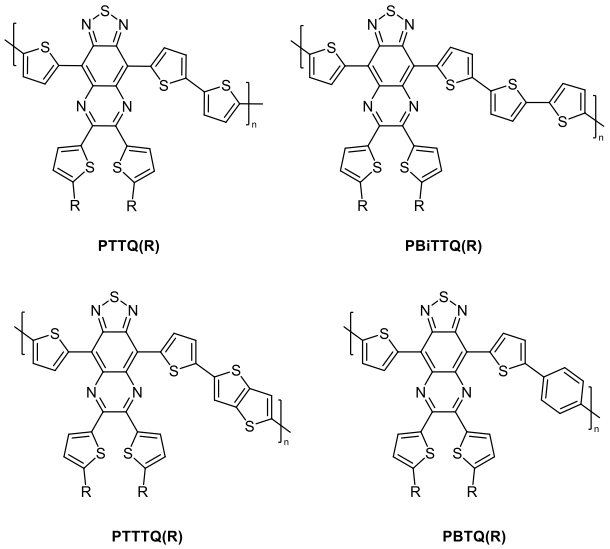

Figure 1. *Overview of the chemical structures of the synthesized polymers*.

The UV-VIS-NIR absorption features of the TQ-based copolymers in solution, together with their absorption coefficients in thin film, are depicted in **Figure 2** and **Table 1**. The absorption coefficients were obtained *via* an integrating sphere setup in which the absorption and reflection/scattering spectra are determined, without taking the very weak interference effects into account. The reported values are averages for three different film thicknesses. The TQ polymers have relatively high absorption coefficients, within the expected range for organic semiconductors. Furthermore, it is clear that **PBTQ(OD)** has (by far) the highest optical gap because of the quite weak electron donating properties of the phenylene bridging units. Incorporation of the more electron rich thiophene-based moieties results in both a broader absorption window and a shift of the absorption onset towards higher wavelengths, affording polymers which absorb in the NIR region from 800 till 1400 nm. Moreover, for some polymers a significant influence of the alkyl side chain length on the absorption spectrum is observed. For the **PTTQ** series, a slight red-shift (both in dilute solution and thin film) can be observed when the side chain length decreases, which likely originates from a more pronounced aggregation. Additionally, an important increase in the absorption coefficient is noticed when the size of the alkyl side chains is reduced. We attribute this to a more efficient packing of the polymers with shorter alkyl chains, resulting in a higher density of conjugated backbones for a specific film thickness.

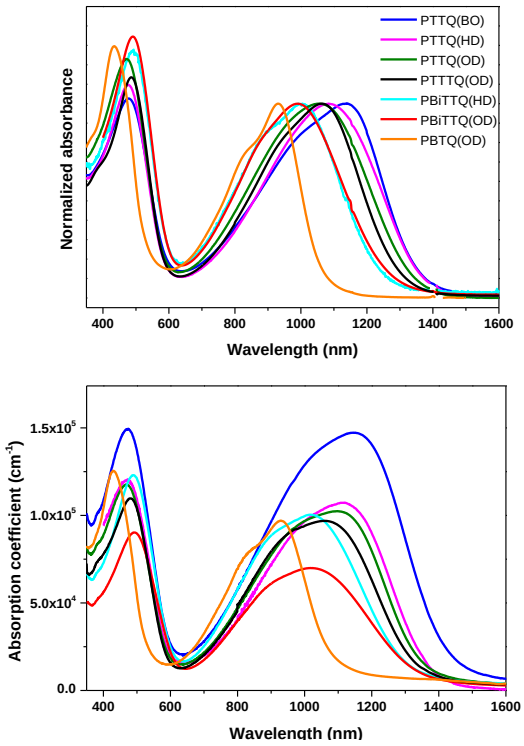

Figure 2. *(top) UV-VIS-NIR absorption spectra of the TQ-based copolymers in chlorobenzene solution and (bottom) the respective absorption coefficients in thin film.*

Table 1. *Molar mass (distributions), optical and electrochemical properties of all TQ-based polymers.*

Polymer	M_n[a] (kDa)	$Đ$	$\lambda_{max\ IR,\ film}$[b] (nm)	E_{red}[c] (V)	E_{ox}[c] (V)	E_{LUMO}[d] (eV)	E_{HOMO}[d] (eV)	$E_{g,opt}$[e] (eV)
PTTQ(BO)	36.6	2.6	1145	-1.10	-0.04	-3.82	-4.87	0.87
PTTQ(HD)	52.8	2.7	1117	-1.09	0.01	-3.82	-4.92	0.91
PTTQ(OD)	21.9	2.0	1111	-1.04	0.07	-3.87	-4.97	0.93
PTTTQ(OD)	64.6	1.8	1053	-1.11	0.17	-3.80	-5.08	0.94
PBiTTQ(HD)	11.1	2.1	1015	-1.11	0.11	-3.80	-5.02	0.95
PBiTTQ(OD)	37.2	2.3	1018	-1.11	0.15	-3.80	-5.06	0.95
PBTQ(OD)	33.1	3.2	930	-1.09	0.39	-3.82	-5.29	1.14

[a] Determined by size exclusion chromatography at 160 °C in 1,2,4-trichlorobenzene (see Figure S3).
[b] Films were prepared by spin-coating a polymer solution from *o*-dichlorobenzene onto a glass substrate.
[c] Onset potentials vs Fc/Fc^+.
[d] Determined from the onset of oxidation/reduction in cyclic voltammetry.
[e] Optical gap, determined from the onset of the solid-state VIS-NIR spectrum.

The frontier orbital energy levels of all polymers were estimated *via* cyclic voltammetry, from the onset of the oxidation and reduction peaks, respectively (see **Figure S1,2**). The oxidation and reduction waves for all polymers are quasi-reversible and the reported values are the means of the first three redox cycles (**Table 1**). From these results it can be observed that the variation of the bandgap due to modification of the electron rich monomers is almost entirely caused by a shift in the position of the highest occupied molecular orbital (HOMO) energy levels. The lowest unoccupied molecular orbital (LUMO) energy levels are mainly determined by the TQ unit, resulting in very similar values for all materials (~-3.8 eV). This should provide sufficient LUMO-LUMO offset with the envisaged electron acceptor $PC_{71}BM$ ([6,6]-phenyl-C_{71}-butyric acid methyl ester), assuring efficient exciton dissociation in bulk heterojunction photodiodes.

The photodetector performance of the novel polymers was evaluated in OPD devices fabricated in the inverted configuration ITO/ZnO/polymer:$PC_{71}BM$/MoO_x/Ag. For all materials, a 1:3 polymer:$PC_{71}BM$ ratio appeared to be optimal and 3 vol% 1,8-diiodooctane (DIO) was added to the active layer blend solution to optimize the blend morphology. Active layer thicknesses were varied with a focus on decreasing the dark current density due to its profound effect on the final detectivity.[7] The dark current-voltage curves and EQEs (measured at -2 V bias) of the corresponding NIR-OPD devices are depicted in **Figure 3**.

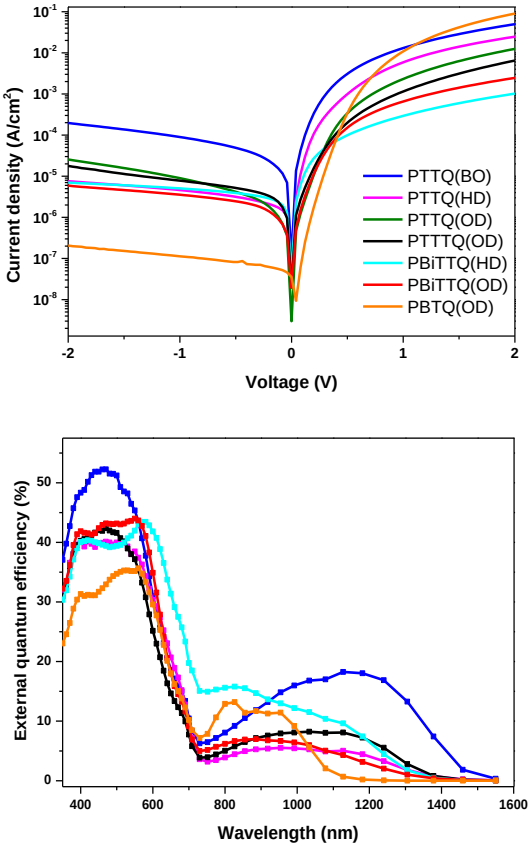

Figure 3. (top) *Current-voltage curves under dark conditions and (bottom) EQE spectra measured at -2 V for the NIR-OPDs based on the respective TQ copolymers.*

From **Figure 3** it is evident that the dark currents differ significantly and they are all relatively high with respect to the devices containing wider bandgap analogues, which were reported to reach values below 1 nA/cm^2.[9] This is an inevitable feature of NIR-OPDs prepared from ultra-low bandgap donor polymers as the increased HOMO energy levels of the electron donor materials increase the chance of charge carrier injection from the electrodes into the active layer.[45] Furthermore, the decreased charge transfer gap ($HOMO_{polymer} - LUMO_{PC71BM}$) increases the chance of thermal charge generation at the interface. These phenomena set a theoretical maximum to the achievable dark current and are an additional hurdle for NIR-OPDs beyond 1 µm to overcome.[38] This hypothesis is supported by the very low dark current density observed for the OPD from the highest gap material **PBTQ(OD)**, with a value of 2×10^{-7} A/cm^2 at -2 V, which is a factor 30 lower than its next competitor **PBiTTQ(OD)**. The highest dark current was obtained for the lowest gap material **PTTQ(BO)**.

Remarkably, the opposite trend is observed in the EQE (and responsivity) spectra, in which the lowest gap material **PTTQ(BO)** showed the highest EQE, with an impressive peak value of 18% at 1130 nm under -2 V bias and a photoresponse up to 1500 nm (**Figure 3**). The highest gap material **PBTQ(OD)**, on the other hand, afforded a photoresponse up to 1100 nm with an EQE exceeding 10% from 800–950

nm. The spectral responsivity (determined from the EQE, see **Figure S4,5**) expresses the output current to the input light power. An increase in responsivity is observed when an external bias is applied as the generated charges are extracted more efficiently. Unfortunately, the EQE (and accordingly the responsivity) of the **PTTQ(OD)**-based OPD device was relatively low and the spectrum was too noisy to be reliable. Further investigation with atomic force microscopy (AFM) showed that this could possibly be attributed to phase separation and a high roughness of the active layer. All other polymers show a favourable blending and relatively low surface roughness (**Figure S6**).

The frequency response (bandwidth) of the **PBTQ(OD)** and **PTTQ(HD)**-based devices was determined via a spectrum analyser (540 nm laser light in combination with a waveform generator enabling to modify the frequency of the light pulsation) (**Figure S7**). It can be observed that the cut-off frequency is in the order of 1 MHz. Since comparison with a Si reference diode produces a similar result, it can be concluded that the measurement is limited by the cut-off frequency of the laser source and that the OPD device has a bandwidth above 1 MHz. The linear dynamic range (LDR) of the **PBTQ(OD)**-based device was also determined (**Figure 4**) and spans over 9 orders of magnitude.

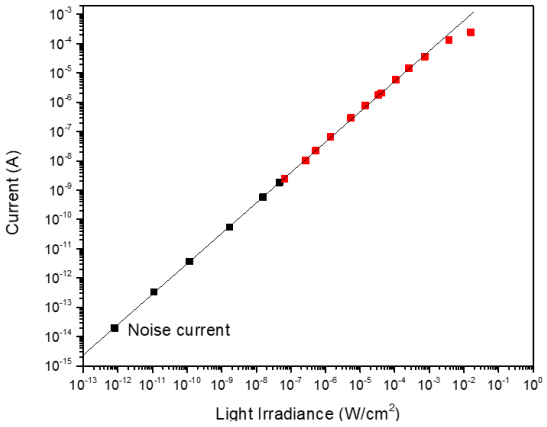

Figure 4. *Linear dynamic range for the **PBTQ(OD)**-based OPD device.*

For photodetectors, the main figure of merit is the specific detectivity, which is governed by the EQE and dark current. The specific detectivity is measured at -2 V and at sufficient high frequencies at which one can assume that shot noise is the dominant contribution to noise. In that case, the specific detectivity can be calculated according to the following equation, in which *q* is the elementary charge of an electron, λ is the incident wavelength, *h* is Planck's constant and *c* is the speed of light:

$$D^* = \frac{EQE\sqrt{q}\lambda}{hc\sqrt{2J_D}} \qquad \text{Eq. 1}$$

The resulting specific detectivities (at -2 V bias) for all optimized NIR-OPDs are depicted in **Figure 5**. The high EQE for the device made from **PTTQ(BO)** is accompanied by a high dark current, affording a specific detectivity above 10^{10} Jones up to 1400 nm. The low dark current for the photodetector based on **PBTQ(OD)**, on the other hand, results in the highest specific detectivity achieved within the series, with a value exceeding 10^{11} Jones in the spectral region of 350−1050 nm. For all other polymer PDs, the detectivities are very similar and exceed 10^{10} Jones from 900−1250 nm, with a peak specific detectivity above 1000 nm. To the best of our knowledge, these values are among the highest reported so far for photodetection with organic/polymer photoactive materials beyond 1 µm.

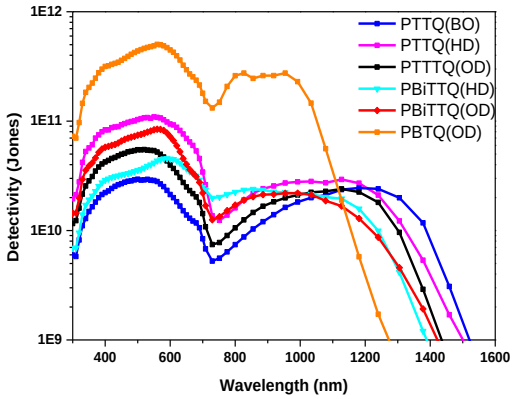

Figure 5. *Shot noise limited specific detectivities (vs wavelength) of the optimized NIR-OPD devices measured at -2 V bias.*

Conclusions

In this report, [1,2,5]thiadiazolo[3,4-*g*]quinoxaline (TQ) was shown to be an excellent building block to develop near-infrared sensitive copolymers for photodetection up to 1.5 µm. Three different TQ monomers were synthesized and copolymerized with carefully selected electron donating monomers to afford a total of seven push-pull copolymers. The prototype photodetectors prepared from **PBTQ(OD)** (in combination with $PC_{71}BM$) showed the highest specific detectivity, exceeding 10^{11} Jones from 350−1050 nm, in line with the higher optical gap for this donor polymer (and concomitant lower dark current density). The device based on the polymer with the most red-shifted absorption, **PTTQ(BO)**, afforded a photoresponse up to 1500 nm and a high external quantum efficiency of 18% at 1130 nm under -2 V bias. The resulting specific detectivity exceeded 10^{10} Jones up to 1400 nm. The specific detectivity of the other NIR-OPDs was above 10^{10} Jones from 900−1250 nm, with a maximum detectivity beyond 1 µm.

Acknowledgements

The authors thank Drs. Christina Kaiser (Swansea University) for her contribution to the frequency response and LDR measurements. F.V., S.G. and J.R. acknowledge the Research Foundation – Flanders (FWO Vlaanderen) for granting them a PhD fellowship. P.V. is a postdoctoral fellow of the FWO Vlaanderen. K.V. and W.M. are grateful for project funding by the FWO (G0D0118N and G0B2718N). Hasselt University and IMOMEC are partners in the SBO project MIRIS (Monolithic Infrared Image Sensors), supported by VLAIO (Vlaams Agentschap Innoveren en Ondernemen). The authors thank Dr. Geert Pirotte for his contribution to this project.

References

1 R. Eckstein, N. Strobel, T. Rödlmeier, K. Glaser, U. Lemmer and G. Hernandez-Sosa, *Adv. Opt. Mater*, 2018, **6**, 1701108.
2 R. D. Jansen-van Vuuren, A. Armin, A. K. Pandey, P. L. Burn and P. Meredith, *Adv. Mater.*, 2016, **28**, 4766–4802.
3 Q. Li, Y. Guo and Y. Liu, *Chem. Mater.*, 2019, **31**, 6359–6379.
4 M. Biele, C. Montenegro Benavides, J. Hürdler, S. F. Tedde, C. J. Brabec and O. Schmidt, *Adv. Mater. Technol.*, 2019, **4**, 1800158.

5 X. Gu, Y. Zhou, K. Gu, T. Kurosawa, Y. Guo, Y. Li, H. Lin, B. C. Schroeder, H. Yan, F. Molina-Lopez, C. J. Tassone, C. Wang, S. C. B. Mannsfeld, H. Yan, D. Zhao, M. F. Toney and Z. Bao, *Adv. Energy Mater.*, 2017, **7**, 1602742.
6 P. Peumans, A. Yakimov and S. R. Forrest, *J. Appl. Phys.*, 2003, **93**, 3693–3723.
7 A. Armin, M. Hambsch, I. K. Kim, P. L. Burn, P. Meredith and E. B. Namdas, *Laser Photon. Rev.*, 2014, **8**, 924–932.
8 D. Yang and D. Ma, *Adv. Opt. Mater.*, 2019, **7**, 1800522.
9 M. Kielar, O. Dhez, G. Pecastaings, A. Curutchet and L. Hirsch, *Sci. Rep.*, 2016, **6**, 39201.
10 A. Rogalski, *Prog. Quantum. Electron.*, 2003, **27**, 59–210.
11 A. Rogalski, *Infrared Phys. Technol.*, 2002, **43**, 187–210.
12 C. M. Lochner, Y. Khan, A. Pierre and A. C. Arias, *Nat. Commun*., 2014, **5**, 5745.
13 X. Yi, F. Wang, W. Qin, X. Yang and J. Yuan, *Int. J. Nanomed.*, 2014, **9**, 1347–1365.
14 P. K. Jain, X. Huang, I. H. El-Sayed and M. A. El-Sayed, *Acc. Chem. Res.*, 2008, **41**, 1578–1586.
15 S. Yoon, K. M. Sim and D. S. Chung, *J. Mater. Chem. C*., 2018, **6**, 13084-13100.
16 M. Binda, D. Natali, A. Iacchetti and M. Sampietro, *Adv. Mater.*, 2013, **25**, 4335–4339.
17 A. M. Smith, M. C. Mancini and S. Nie, *Nat. Nanotechnol.*, 2009, **4**, 710–711.
18 C. Downs and T. Vandervelde, *Sensors*, 2013, **13**, 5054–5098.
19 N. Gasparini, A. Gregori, M. Salvador, M. Biele, A. Wadsworth, S. Tedde, D. Baran, I. McCulloch and C. J. Brabec, *Adv. Mater. Technol.*, 2018, **3**, 1800104.
20 S. Park, K. Fukuda, M. Wang, C. Lee, T. Yokota, H. Jin, H. Jinno, H. Kimura, P. Zalar, N. Matsuhisa, S. Umezu, G. C. Bazan and T. Someya, *Adv. Mater.*, 2018, **30**, 1802359.
21 Y. Yao, Y. Liang, V. Shrotriya, S. Xiao, L. Yu and Y. Yang, *Adv. Mater.*, 2007, **19**, 3979–3983.
22 X. Gong, M.-H. Tong, S. H. Park, M. Liu, A. Jen and A. J. Heeger, *Sensors*, 2010, **10**, 6488–6496.
23 X. Zhou, D. Yang and D. Ma, *Adv. Opt. Mater.*, 2015, **3**, 1570–1576.
24 S. Xiong, J. Tong, L. Mao, Z. Li, F. Qin, F. Jiang, W. Meng, T. Liu, W. Li and Y. Zhou, *J. Mater. Chem. C*, 2016, **4**, 1414–1419.
25 S. Shafian, H. Hwang and K. Kim, *Opt. Express.,* 2016, **24**, 25308–25316.
26 G. Simone, D. Di Carlo Rasi, X. de Vries, G. H. L. Heintges, S. C. J. Meskers, R. A. J. Janssen and G. H. Gelinck, *Adv. Mater.*, 2018, **30**, 1804678.
27 D. W. Lee, Y. Kang, B. H. Jo, G. G. Jeon, J. Park, S. E. Yoon, J. Zheng, T. K. Ahn, H. J. Park, B.-G. Kim and J. H. Kim, *Org. Electron.*, 2019, **64**, 274–279.
28 T. Hasegawa, M. Ashizawa, J. Hiyoshi, S. Kawauchi, J. Mei, Z. Bao and H. Matsumoto, *Polym. Chem.*, 2016, **7**, 1181–1190.
29 J. Fan, J. D. Yuen, M. Wang, J. Seifter, J.-H. Seo, A. R. Mohebbi, D. Zakhidov, A. Heeger and F. Wudl, *Adv. Mater.*, 2012, **24**, 2186–2190.
30 K. Wang, J. Huang, J. Ko, W. L. Leong and M. Wang, *J. Polym. Sci.,* 2017, **55**, 3205–3213.
31 X. Cao, J. Tong, Z. He, M. Zhang, X. Zhang, J. Ma, P. Gao, J. Li, P. Zhang, C. Wang, Y. Xia and H. Wu, *Dyes Pigm.*, 2018, **158**, 319–325.
32. J. Han, D. Yang, D. Ma, W. Qiao and Z. Y. Wang, *Adv. Opt. Mater.*, 2018, **6**, 1800038.
33 F. Verstraeten, S. Gielen, P. Verstappen, J. Kesters, E. Georgitzikis, J. Raymakers, D. Cheyns, P. Malinowski, M. Daenen, L. Lutsen, K. Vandewal and W. Maes, *J. Mater. Chem. C*, 2018, **6**, 11645–11650.
34 X. Gong, M. Tong, Y. Xia, W. Cai, J. S. Moon, Y. Cao, G. Yu, C.-L. Shieh, B. Nilsson and A. J. Heeger, *Science*, 2009, **325**, 1665–1667.
35 L. Zheng, T. Zhu, W. Xu, L. Liu, J. Zheng, X. Gong and F. Wudl, *J. Mater. Chem. C*, 2018, **6**, 3634-3641.
36 A. E. London, L. Huang, B. A. Zhang, M. B. Oviedo, J. Tropp, W. Yao, Z. Wu, B. M. Wong, T. N. Ng and J. D. Azoulay, *Polym. Chem.*, 2017, **8**, 2922–2930.
37 Z. Wu, Y. Zhai, W. Yao, N. Eedugurala, S. Zhang, L. Huang, X. Gu, J. D. Azoulay and T. N. Ng, *Adv. Funct. Mater.*, 2018, **28**, 1805738.
38 Z. Wu, W. Yao, A. E. London, J. D. Azoulay and T. N. Ng, *Adv. Funct. Mater.,* 2018, **28**, 1800391.

39 E. Perzon, F. Zhang, M. Andersson, W. Mammo, O. Inganäs and M. R. Andersson, *Adv. Mater.*, 2007, **19**, 3308–3311.
40 T. T. Steckler, P. Henriksson, S. Mollinger, A. Lundin, A. Salleo and M. R. Andersson, *J. Am. Chem. Soc.*, 2014, **136**, 1190–1193.
41 J. Qi, X. Zhou, D. Yang, W. Qiao, D. Ma and Z. Y. Wang, *Adv. Funct. Mater.*, 2014, **24**, 7605–7612.
42 J. Lee, S.-J. Ko, H. Lee, J. Huang, Z. Zhu, M. Seifrid, J. Vollbrecht, V. V. Brus, A. Karki, H. Wang, K. Cho, T.-Q. Nguyen and G. C. Bazan, *ACS Energy Lett.*, 2019, **4**, 1401–1409.
43 L. Hu, J. Han, W. Qiao, X. Zhou, C.-L. Wang, D. Ma, Y. Li and Z. Y. Wang, *Polym. Chem.*, 2018, **9**, 327–334.
44 S. Xu, E. H. Kim, A. Wei and E. Negishi, *Sci. Technol. Adv. Mater.*, 2014, **15**, 044201.
45 G. Simone, M. J. Dyson, C. H. L. Weijtens, S. C. J. Meskers, R. Coehoorn, R. A. J. Janssen and G. H. Gelinck, *Adv. Optical Mater.*, 2019, **8**, 1901568.